Evidence for a Strong Association of Short-Duration Intense Rainfall with Urbanization in the Beijing Urban Area

PING YANG

China Meteorological Administration Training Center, Beijing, and Department of Atmospheric Science, School of Environmental Studies, China University of Geosciences, Wuhan, and Institute of Urban Meteorology, China Meteorological Administration, Beijing, China

GUOYU REN

Department of Atmospheric Science, School of Environmental Studies, China University of Geosciences, Wuhan, and Laboratory for Climate Studies, National Climate Center, China Meteorological Administration, Beijing, China

PENGCHENG YAN

Institute of Arid Meteorology, China Meteorological Administration, Lanzhou, China

(Manuscript received 9 September 2016, in final form 11 April 2017)

ABSTRACT

Correlations of the urban heat island intensity (UHII) and key surface variables with the short-duration intense rainfall (SDIR) events are examined for the Beijing urban areas by applying hourly data of a high-density automatic weather station (AWS) network. Higher frequencies (amounts) of the SDIR events are found in or near the central urban area, and most of the SDIR events begin to appear in late evening and nighttime, but tend to end in late night and early morning. Correlations of the UHII with the SDIR frequency (amount) are all highly significant for more than 3 h ahead of the beginning of the SDIR events. Although the UHII at immediate hours (<3 h) before the SDIR occurrence is more indicative of SDIR events, their occurrence more depends on the magnitude of the UHII at earlier hours. The UHII before the beginning of the SDIR events also shows high-value centers in the central urban area, which is generally consistent with the distribution of the SDIR events. The spatial and temporal patterns of regional SDIR events exhibit similar characteristics to the site-based SDIR events and also show a good relationship with the UHII in the urban areas. In addition to the UHII over the urban areas, surface air temperature, surface air pressure, relative humidity, and near-surface wind directions at the Beijing station experience large changes before and after the beginning time of regional SDIR events, and have the potential to indicate the occurrence of SDIR events in the studied area.

1. Introduction

Studies have indicated that the local climates of urban areas are significantly different from their nearby suburbs (Oke 1982; Seto and Shepherd 2009; Yang et al. 2013b; Ren and Zhou 2014). The huge modification of land surface and atmospheric boundary layers in urban areas has an obvious effect on near-surface climate by changing the energy and water balance (Oke 1976, 1987; Kalnay and Cai 2003; Ren et al. 2008; Shepherd et al. 2010). The alternation of surface heat budget forms the urban heat island (UHI), rendering the city consistently warmer than its surroundings (Stewart and Oke 2012; Yang et al. 2013b). The most pronounced UHIs have been observed for some large cities on calm and clear winter nights (Jáuregui 1973; Rosenzweig et al. 2005). It is also demonstrated that the UHI intensity exhibits diurnal and seasonal variation, modulated by synoptic weather conditions. The UHI in urban areas produces rising and subsiding air, resulting in local UHI circulation (Arnfield 2003; Han et al. 2014).

Precipitation in megacities draws attention because of its potential great impacts on urban management of flash floods, waterlogging, landslides, and mudflows. Studies show that urbanization can lead to an increase in total precipitation in downtown and downwind areas in big

Corresponding author: Guoyu Ren, guoyoo@cma.gov.cn

DOI: 10.1175/JCLI-D-16-0671.1

cities (Changnon 1979; Han et al. 2014; Zhong et al. 2015). During the past several decades, both abundant observations and climate model simulations show the evidences for the relationship between urbanization and precipitation (e.g., Changnon 1968, 1979; Huff 1986; Oke 1988; Hennessy et al. 1997; Allen and Ingram 2002). Changnon et al. (1991) analyzed dense precipitation data in St. Louis, Missouri, and found that urban effect leads to an increasing precipitation of 17% and 4% in autumn and spring, respectively. Recent observational studies presented more evidences that the urbanization process does affect the spatial distribution and the amount of precipitation, and that precipitation tends to be enhanced over urban areas (Rosenfeld 2000; Sun and Shu 2007; Zhou and Ren 2009; Miao et al. 2011; Liang et al. 2013; Pathirana et al. 2014; Dou et al. 2015; Chen et al. 2015). Mishra et al. (2012) studied the 100 largest urban regions together with their surrounding nonurban areas and demonstrated a spatially mixed picture for precipitation-related changes resulted from urbanization across the continental United States. Dou et al. (2015) analyzed the correlation between UHIs and summer rainfall and found that strong UHIs could induce or enhance thunderstorm formation.

Because of the huge damage caused by heavy rainfall in cities, more and more research has been focused on the effect of urbanization on extreme rainfall events. Storm bifurcation was first noted in New York City in analysis of radar measurements by Bornstein and LeRoy (1990). Kishtawal et al. (2010) found apparent rising trends in the frequency of precipitation over highly urbanized regions of India. Lin et al. (2011) reported that a typical precipitation system over northern Taiwan tended to be stronger in urban areas than in nonurban areas. Pathirana et al. (2014) examined the relations between city size and extreme precipitation intensity and found that 75% of tropical cities exhibited obvious reinforcement in extreme rainfall events. Shastri et al. (2015) demonstrated overall characteristics of the impacts of urbanization on summer extreme precipitation in India, and found that urbanization has significant effects on extreme rainfall events in the central and western regions of the country.

A few mechanisms were proposed to explain the relations of urbanization and precipitation anomalies. Studies indicated that the UHI is a low-level heat source in the atmosphere that could generate convection, and the higher roughness and anthropogenic aerosols could be two other factors affecting urban precipitation (Han et al. 2014). Numerical models were also used to investigate the UHI-induced local flows, showing that the intensity and horizontal structure of UHI could affect the amount and spatial pattern of precipitation (Lin and Smith 1986; Craig and Bornstein 2002; Han and Baik 2008; Ochoa et al. 2015). Studies indicated that larger roughness in urban areas can enhance precipitation (e.g., Thielen et al. 2000), while other research found that the larger roughness could increase the convergence on the windward side of city, which is not strong enough to induce storms (Rozoff et al. 2003). Increasing aerosols in urban environments could noticeably affect the development of clouds and precipitation (Diem and Brown 2004; Mölders and Olson 2004; Ochoa et al. 2015). In spite of the previous work, the role of disrupted convective systems or aerosols in modifying precipitation over, or downwind of, urban areas still needs further investigation.

The current population of Beijing Municipality (BJM) reaches almost 20 million. As a megacity, the Beijing urban area, as delineated by the Sixth Ring Road, has been expanded to about 2200 km. The large and rapid change of urban environment might affect total and intense precipitation of the urban areas. Some studies showed that intense precipitation is more likely to occur during the period from late afternoon to early morning the next day in Beijing due to urbanization (Li et al. 2008; Yang et al. 2013a; Song et al. 2014), despite the fact that no consensus has been reached as to the specifically spatial pattern of the urban-induced intense precipitation frequency (Wu et al. 2000; Yu et al. 2007). Other research, for example by using regional climate models, indicated that urbanization could be beneficial to a general reduction of precipitation, particularly in regions downwind of the urban areas (e.g., Zhang et al. 2009, 2014). It is therefore clear that the temporal and spatial characteristics of the urban-induced precipitation and intense rainfall over Beijing are still controversial. One of the main reasons for the inconsistency is that the previous studies are mainly based on the observational data obtained from only a few scattered national meteorological stations.

In addition, because Beijing's topography is varied and complicated, the external mechanisms of precipitation in different area over Beijing are similarly varied. The previous research, especially for precipitation, usually aimed at the whole area of BJM (Yang et al. 2013a, 2017), the scale of which is still too large. Thus, the descriptions of tiny variation and differences inside key regions such as inside the Sixth RR are lacking. More detailed research will provide more information and be useful to develop a better understanding of the urban intense precipitation. Besides, the previous analyses of the possible effect of urbanization on precipitation were also mostly focused on summer total rainfall, while the features of extreme precipitation, such as the persistence, intensity, and spatial structure of short-duration intense rainfall events, have not received enough attention. Moreover, few investigations have been made so far to examine the feedbacks from the short-duration intense rainfall to other urban climatic variables, including the UHI intensity.

Therefore, it is necessary to further investigate more detailed characteristics of urbanization-related intense precipitation events and their feedbacks to other climatic variables in the urban and surrounding areas of Beijing City, which are important for understanding the urban precipitation process and the accurate prediction of weather and climate of the megacity.

The purpose of this paper is therefore to examine the climatological characteristics of the short-duration intense rainfall events in Beijing urban areas, and the relationships between the UHI and urban heavy rainfall events by analyzing the hourly data of automatic weather stations (AWS). It will also make an attempt to explore the possible influential factors of site-recorded and regional short-duration intense rainfall events.

2. Study area, data, and methods

a. Study area

Beijing Municipality comprises a total area of about 1.6 million square kilometers. It is located at the northern end of the North China Plain, south of the Yan Shan Mountains. The southeast region is geographically connected with Tianjin, and the rest is surrounded by Hebei Province. The flat southeast area occupies roughly 38%; the remaining northwest area is mostly mountainous. The elevations of the plain area range from 20 to 80 m above mean sea level (MSL). Climatologically, Beijing has a typical monsoon-driven semihumid to humid continental climate, with a hot and humid summer and a cold and dry winter. Taking the period 2007–14 for example, the mean annual precipitation amount of Beijing is 539.3 mm, and the hot humid summer in Beijing results from warm and humid monsoon winds from the south, bringing Beijing most (66%) of its annual precipitation (Yang et al. 2017).

With the rapid economic growth and urbanization, population in Beijing City undergoes a fast increase and over half of the population lives in the urban areas. So far, a multiple Ring Road (RR) system of transportation (Fig. 1) has been developed in the urban zones (Yang et al. 2013b). The Fourth, Fifth, and Sixth RRs were opened successively in 2001, 2003, and 2009, with lengths of 65.3, 98.6, and 187.6 km respectively. The areas inside different RRs actually represent different levels of urbanization with varied densities of population and buildings as well. In this study, the stations located inside the Sixth RR in Beijing are regarded as urban sites, and those inside the Fourth RR as central urban sites (Fig. 1). Beijing Observatory (BO) is also shown as a representative national station and is marked by a red plot in Fig. 1.

b. Observational data

In this study, data of the observed hourly surface air temperature and rainfall amount collected from 115 stations in Beijing for the time period 2007–14 were obtained from the Meteorological Information Center, Beijing Meteorological Bureau (MIC/BMB). The data have been preliminarily quality-controlled by the MIC, and the possibly wrong records have been checked and corrected by applying a method of regionally climatological extreme-value thresholds (Ren and Xiong 2007; Ren et al. 2015). To increase the robustness of our analysis, the data are checked and data controlled once more using the methods by Yang et al. (2011) and Yang and Liu 2013). The methods of the extreme-value thresholds and manual identification are both applied in checking data.

Based on the historic observational data of manual measurements and the regional feature of precipitation in BJM, different seasons have different thresholds of extreme-value (thresholds are determined as 50, 80, 50, and 30 mm h^{-1} in spring, summer, fall, and winter, respectively) (Yang et al. 2011, 2013a,b). When an hourly record exceeds its seasonal threshold, it is considered suspicious, and it would be treated as a missing record if proved wrong by comparing the records of the adjacent stations. To minimize the impact of missing records on the analysis, only stations with missing values less than 3% of the total records for the 8 years were selected for use, and the missing data were interpolated by applying the valid data of the nearest five stations (Yang et al. 2013a).

After the quality control of the data, 38 (of 63 total) observational stations evenly distributed inside the Sixth RR were selected for use (Fig. 1) eventually. Seven reference stations (Fig. 1) outside the Sixth RR with similar physiographic characteristics were selected in order to calculate the UHI intensities of the urban stations. The heights of the reference stations are almost the same as those in urban areas. The two sets of data are also used in pairs to compare the precipitation between urban and rural areas. Because of the importance of the reference data series, the seven stations (Table 1) were selected by using a remote sensing–based method, which was developed with a strictly defined standard (Ren and Ren 2011).

Beijing Observatory (also called Beijing Station in some previous publications) is considered as a representative

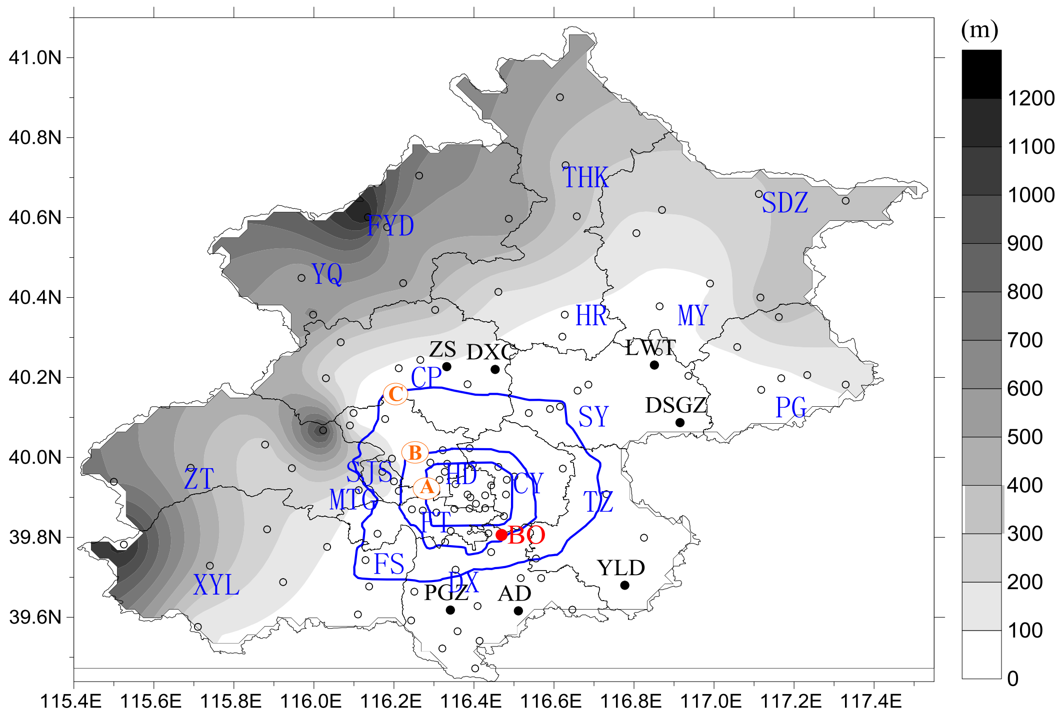

FIG. 1. Site locations (marked by plots), the surface elevations (marked by isograms) and distribution of ring roads (RRs; marked by blue closed circles named A to C, which represent the Fourth to Sixth RRs) in the whole area of Beijing Municipality. The abbreviations marked in blue are for representative stations of Beijing Municipality: SY = Shun Yi, HD = Hai Dian, YQ = Yan Qing, FYD = Fo Ye Ding, THK = Tang He Kou, MY = Mi Yun, HR = Huai Rou, SDZ = Shang Dian Zi, PG = Ping Gu, CY = Chao Yang, CP = Chang Ping, ZT = Zhai Tang, MTG = Men Tou Gou, BO = Beijing Observation (marked by a red dot), SJS = Shi Jing Shan, FT = Feng Tai, DX = Da Xing, FS = Fang Shan, XYL = Xia Yun Ling). The abbreviations marked in black plots outside of the Sixth RR are for seven rural stations: FHL = Feng Huang Ling, YLD = Yong Le Dian, PGZ = Pang Ge Zhuang, AD = An Ding, NZ = Nan Zhao, DXC = Dong Xin Cheng, DSGZ = Da Sun Ge Zhuang, and LWT = Long Wan Tun.

station of Beijing in the study. The observed hourly wind speed, wind direction, surface air pressure, and relative humidity data, together with the synoptic process records, from the BO are used to represent the characteristics of relevant meteorological elements for the whole study area.

c. *Analysis methods*

In the study, UHI intensity (UHII) is defined as the temperature difference between urban and suburban areas. The rural temperature (T_r) is the mean temperature value of the seven reference stations, while the urban temperature (T_u) is the temperature of any individual urban station, or the mean values of urban stations inside any specific urban areas. The UHII (ΔT_{u-r}) can be thus obtained by the following formula:

$$\mathrm{UHII} = \Delta T_{u\text{-}r} = T_u - T_{r}. \tag{1}$$

The type of rainfall event in this study is restricted to short-duration intense rainfall (SDIR). SDIR for a

TABLE 1. Basic information of seven reference stations.

Abbrev. (station name)	Location [lat. (N), lon. (E)]	Elevation (m)	Elevation difference from urban areas (m)
FHL (Fenghuangling)	40.11°N, 116.10°E	73.0	26.1
YLZ (Yonglezhan)	39.68°N, 116.78°E	17.0	−29.9
PGZ (Panggezhuang)	39.62°N, 116.34°E	34.0	−12.9
AD (Anding)	39.62°N, 116.51°E	24.0	−22.9
DXC (Dongxincheng)	40.22°N, 116.45°E	49.0	2.1
DSGZ (Dasungezhuang)	40.09°N, 116.92°E	35.0	−11.9
LWT (Longwantun)	40.23°N, 116.85°E	52.0	5.1
Average	39.90°N, 116.51°E	42.7	−4.2

given station is defined according to the following criteria:

1) a SDIR event begins when hourly rainfall is more than 0.1 mm and ends when it falls below 0.1 mm;
2) the duration of the SDIR event, or the hours between the starting and end time, must be equal to or more than 1 h, and equal to or less than 12 h; and
3) the accumulated amount of the SDIR event, or the total rainfall amount between the beginning and end time, has to reach more than 30 mm.

The above definition of SDIR is used for each single station, which is also named site-based SDIR in this paper. Annual mean SDIR frequency is the average number of SDIR events during 2007–14, and annual mean SDIR amount is the average accumulated amount of the SDIR events during the same period. Zero time is defined as the beginning time of a SDIR event.

To compare the SDIR among different stages of UHII in a day, the four stages of UHII proposed by Yang et al. (2013b) are used, namely a relatively stable high UHII stage [2100 to 0600 local standard time (LST)], a relatively stable low UHII stage (1100 to 1600 LST), a swiftly falling stage (0600 to 1100 LST), and a swiftly rising stage (1600 to 2100 LST).

In addition, the relationship of the spatial pattern of UHII and SDIR is examined in the analysis. The spatial correlation coefficients (r) between UHII and SDIR frequency and amount were calculated using the following formula:

$$r = \frac{\sum_{i=1}^{n}(x_i - \overline{x})(y_i - \overline{y})}{\sqrt{\sum_{i=1}^{n}(x_i - \overline{x})^2}\sqrt{\sum_{i=1}^{n}(y_i - \overline{y})^2}}, \qquad (2)$$

where n is the number of stations in the urban area, x_i is the UHII values for each site, and y_i is the annual frequency or rainfall amount of the SDIR events for each site.

To investigate the specific spatial patterns of UHII before and after the beginning time of the SDIR events, the distributions of UHII at typical moments before and after the beginning time of the SDIR events within 24 h are examined. These moments are 6, 3, and 1 h before the beginning time of the SDIR events (i.e., −6, −3, and −1 h, respectively), and 1, 3, and 6 h after the beginning time of the SDIR events.

The SDIR events mentioned above are the events that occurred at any individual site. In fact, many of the site-based SDIR events actually occurred synchronously at some neighboring stations due to regional or clustering characteristics of precipitation (Yang et al. 2012, 2013c). It is necessary to also account for regional SDIR events, which could be defined based on the site-based SDIR events as follows:

1) the individual site-based SDIR events inside the Sixth RR occur synchronously within one day, and
2) the number of stations undergoing SDIR exceeds 50% of the total stations inside the Sixth RR.

In this case, as the total number of urban stations is 38, when the site-based SDIR events occur synchronously at 19 or more urban stations in a day, it can be recorded as a regional SDIR event. The beginning (end) time of a regional SDIR event is defined as the earliest (latest) time of all the urban stations undergoing the regional SDIR event.

3. Results

a. Spatial and temporal variation of SDIR

Figure 2 shows the spatial distribution of the annual mean frequencies (Fig. 2a) and rainfall amounts (Fig. 2b) of SDIR events in whole area of Beijing during 2007–14. As shown in Fig. 2a, an obvious large-value center of annual mean SDIR frequencies occur in the urban areas and the northeastern mountains. For the spatial distribution of annual mean SDIR amount, similar pattern is observed over the whole area of Beijing Municipality. One large-value center is in the northeastern region of Beijing, including Mi Yun and Ping Gu. This is mainly caused by the interaction between the low-layer prevailing warm-season southwesterly and the geomorphological effect of the mountains. Previous studies showed that the prevailing southwest currents flow over Beijing all year, but particularly in summer (Yang et al. 2017). The fact that upslope southwesterly warm-moist air flows over the mountains in the northeastern center provides favorable conditions for the development of SDIR event. It might be also important that the warm, moist airstream has been heated by the upstream urban land surface and moistened somewhat by evaporation over the Mi Yun Reservoir.

The area inside the Sixth RR is another center with high frequencies and amounts of SDIR events. Different from the mountainous center, the second center is located in the plain region with the average elevation well below 50 m MSL, and it is almost completely within the urban areas. As discussed below, the urban SDIR center has to be explained by the urbanization effect. During the 8-yr period, the annual mean frequency (amount) over the urban area inside Sixth RR is 3.2 occurrences (158.2 mm). The highest value of annual mean frequency appears in Si Hui Qiao, which is marginally located inside the Fourth RR in the east area. The largest

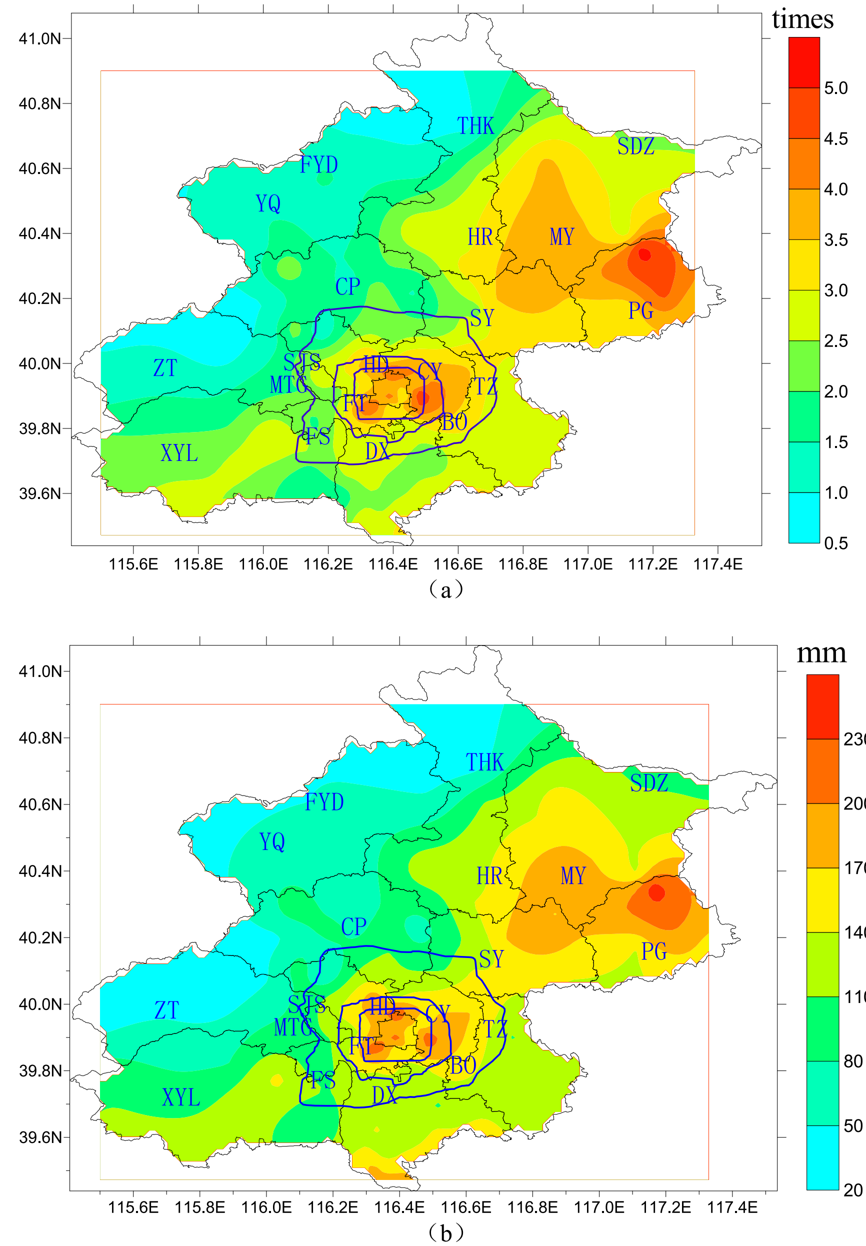

FIG. 2. Spatial distributions of (a) annual mean frequencies and (b) annual mean rainfall amounts of SDIR events in whole area of Beijing during 2007–14. Three blue circles indicate the Fourth to Sixth RRs as shown in Fig. 1 and the abbreviations marked in blue indicate representative stations (listed in Fig. 1).

annual mean amount occurs in Tian An Men, which is located in the center of the region inside Fourth RR. Both of the two high-value points are within or around the Fourth RR, an area that is economically highly developed and demographically densely populated, and one of them is even the center of the whole city. The lowest records of the SDIR frequency and amount are both in a site named Dao Xiang Hu, which is marginally located inside the Sixth RR in the northwest area and is less urbanized. Previous studies have found that larger rainfall amount and heavy rain frequency tend occur in the urban areas, which has been considered an important reason for increasing urban water logging disasters and economic damage (Yu et al. 2007; Yang et al. 2013a). Our analysis of SDIR events confirms the previous findings.

Figure 3 illustrates the obvious differences of annual mean frequencies and rainfall amounts and their

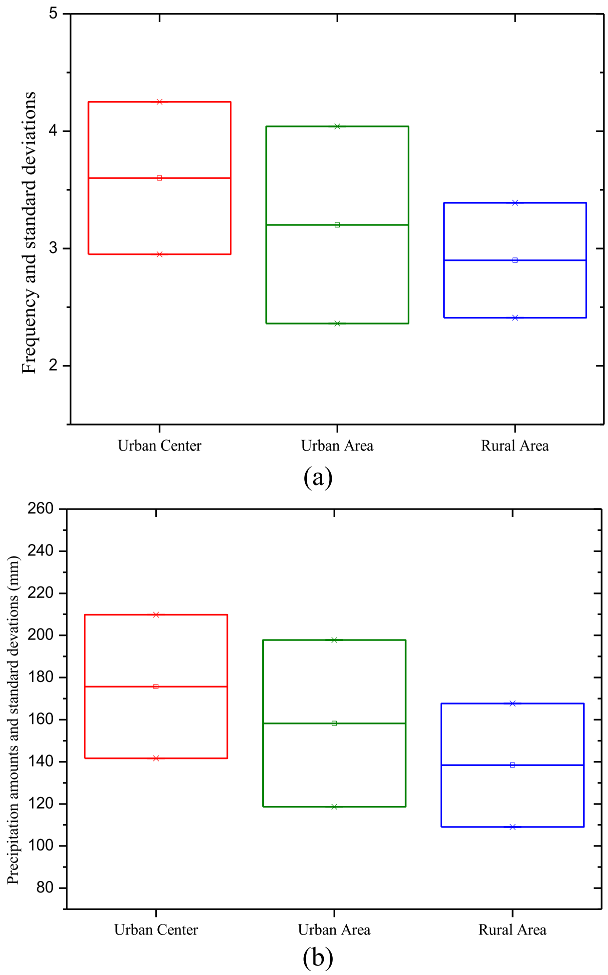

FIG. 3. Annual mean (a) frequencies and (b) rainfall amounts with standard deviations of SDIR events in urban center (red; inside the Fourth RR, including 7 sites), urban area (olive; inside the Sixth RR, including 38 sites) and rural areas (blue; including 7 reference sites). Midlevel lines with a box denote mean values, while the high- and low-level lines with a "×" denote the standard deviation around the mean values.

standard deviations of SDIR events between the urban center (including 7 sites inside the Fourth RR) and the general urban (including 38 sites inside the Sixth RR) and rural areas (including 7 reference sites) . It is clear that more SDIR events occur in the urban area, especially the urban center. The annual mean frequency of SDIR in the urban area (center) is 0.3 (0.7) times more than that in the rural area [3.2(3.6):2.9]. The annual mean rainfall amount of SDIR in urban area is 158.2 mm, 27.6% of the annual total precipitation (573.1 mm), which is also much more than that in the rural area (138.4 mm). It is apparent that the SDIR events more easily occur in the urban areas inside the Sixth RR than in rural regions.

Seasonal and diurnal variations of SDIR in the urban area of BJM are shown in Figs. 4 and 5, respectively. The 10-day mean occurrence frequency, accumulated amount, and intensity of SDIR events are given in Fig. 4, with yellow, cyan, and magenta representing different 10-day periods of a month. The highest values of frequency, amount, and intensity are all in the last 10-day period of July. It is also clear that the largest values of the SDIR indicators take place in summer, from June to August, accounting for more than 90% of the total. Some SDIR events occur in autumn, fewer than that in spring. There is no SDIR event in winter.

There are some detectable differences of seasonal variations among frequency, accumulated rainfall amount, and intensity of SDIR (Fig. 4). First, the top three 10-day periods of SDIR frequencies all fall in July. However, the amount and intensity of SDIR are characterized by a wider seasonal distribution. Consequently, the intensity of two 10-day periods of August even surpasses that of the second 10-day period of July. Second, the frequencies of SDIR events in June are generally higher than those in August, whereas the amount and intensity of SDIR events are mostly the opposite. It is well known that precipitation and rainstorms in Beijing most frequently occur in late July and early August (Li et al. 2008). Although the SDIR amount and intensity exhibit an approximately similar seasonal distribution to rainfall and rainstorms, the frequencies of SDIR events in August are apparently less than those in July. This implies that there is a tendency for more frequent and less intense SDIR events to occur in late July and less frequent and more intense SDIR events to occur in early August.

Diurnal variations of frequency, amount, and intensity of SDIR events with different beginning and end times in the urban area are shown in Fig. 5. Most of the SDIR events begin to occur during the evening and early night from 1600 to 2200 LST. The late night from 0000 to 0600 LST witnesses the second most frequent SDIR events to begin. Fewer SDIR events begin during morning and early afternoon, with the lowest frequency, amount, and intensity seen from 1200 to 1300 LST.

In contrast, the SDIR events generally tend to end in late night and early morning from 0200 to 0700 LST, with those ending around 0400 LST being most frequent. The frequency, amount, and intensity of the SDIR events ending during noontime also is at a low level. It has been demonstrated by previous studies that the UHII during nighttime is more obvious than that during daytime (e.g., Yang et al. 2013b; Liu et al. 2014). Yang et al. (2013b) further classified four categories of diurnal UHII for the urban areas of Beijing, with the swiftest increase of the UHII from 1800 to 2200 LST and

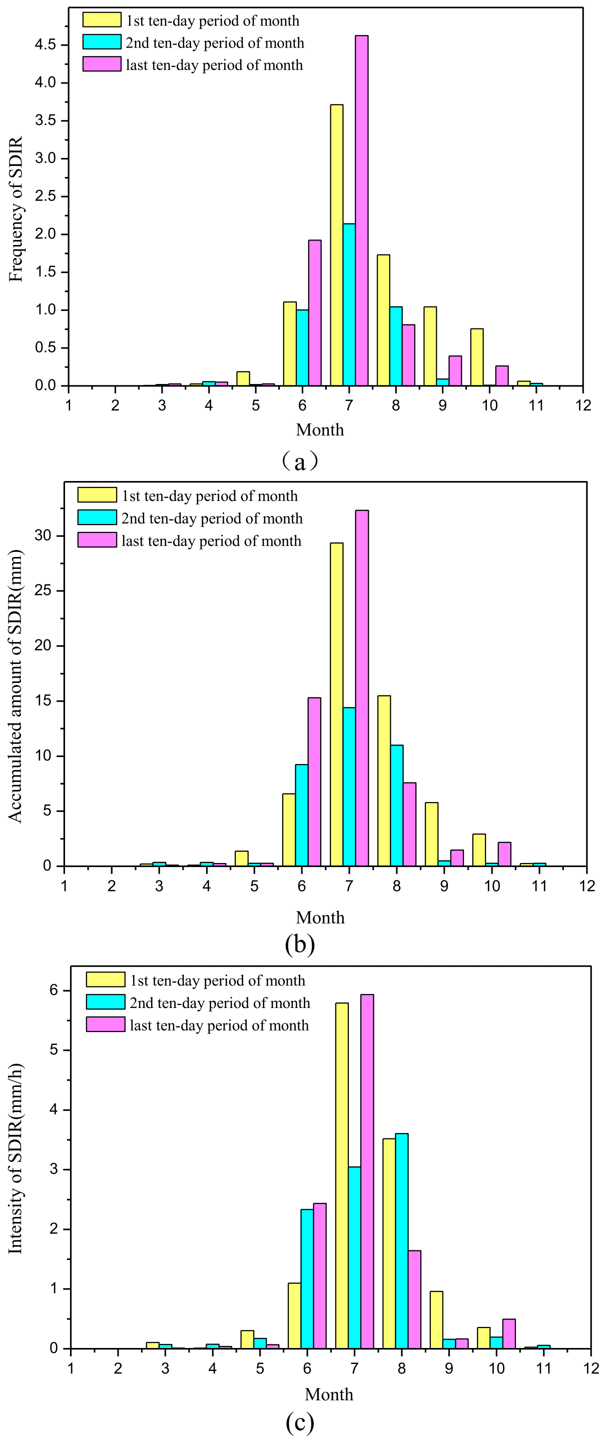

FIG. 4. Seasonal variations of (a) frequency, (b) amount, and (c) intensity of SDIR events in urban areas of Beijing Municipality. Yellow, cyan, and magenta denote the first, second, and last 10-day period of each month, respectively.

the UHII plateau from 2200 to 0600 LST. The marked diurnal variation of the UHII might be a reason for the higher frequency of the SDIR events occurring after sunshine ending during early morning. This possible association of the urban SDIR events with the UHII will be further discussed below.

b. *Relationships between UHII and SDIR*

Variations of the UHII before and after the beginning hours of SDIR events for different urban belts are shown in Fig. 6a. As mentioned above, the beginning time of SDIR event is regarded as zero time. It is obvious from Fig. 6a that all of the UHII curves are separated into two different periods by zero time. For the whole urban area and for each belt, the UHII maintains high values before the zero time, while the values stay relatively low or even become negative after the zero time. The highest value of UHII appears within one hour before the zero time and then it swiftly drops to bottom as a large negative value when the SDIR events beginning. In the 4th and 4th–5th RR zones in particular (hereafter the specific ring roads will be written as Fourth, Fifth, etc., but the zones as 4th, 4th–5th, etc.) the UHII at zero time is the lowest among the total 24 h. Taking the urban area as an example, the UHII keeps a high level around 0.5°C before the SDIR appears and it reaches to peak value of 1.0°C at −1 h, or one hour before the zero time. At the hour when the SDIR events happen, the UHII suddenly drops to a negative value of −1.0°C and then recovers slowly to around 0°C at about 6 h after the beginning of the SDIR events. There is a little difference for 5th–6th RR zone, however, with the lowest UHII lagging zero time an hour, probably due to the fact that the 5th–6th RR zone is less affected by UHI effect.

It is apparent from Fig. 4 that the SDIR events are mostly concentrated in the summer months (June–August). To better understand the association between UHII and SDIR events, the diurnal variation of UHII in different urban belts in summer is shown in Fig. 6b. The summer mean UHII of the whole urban area is 0.89°C, and it is 1.25°, 0.83°, and 0.59°C in the 4th, 4th–5th, and 5th–6th RR zones, respectively. In Fig. 6a, it is seen that the UHII value at −1 h (one hour before zero time) exceeds 1.0°C. It is therefore interesting to note that, before the onset of the SDIR events, the UHII of urban area is generally less changeable for almost 6–8 h, usually around 0.5°C, and then it rapidly rises to a peak value around 1.0°C, exceeding the summer mean UHII. The abrupt UHII increase at about −1 h may imply an enhanced UHI-driven convection in the central urban area, forming an atmospheric condition for inspiriting the SDIR events.

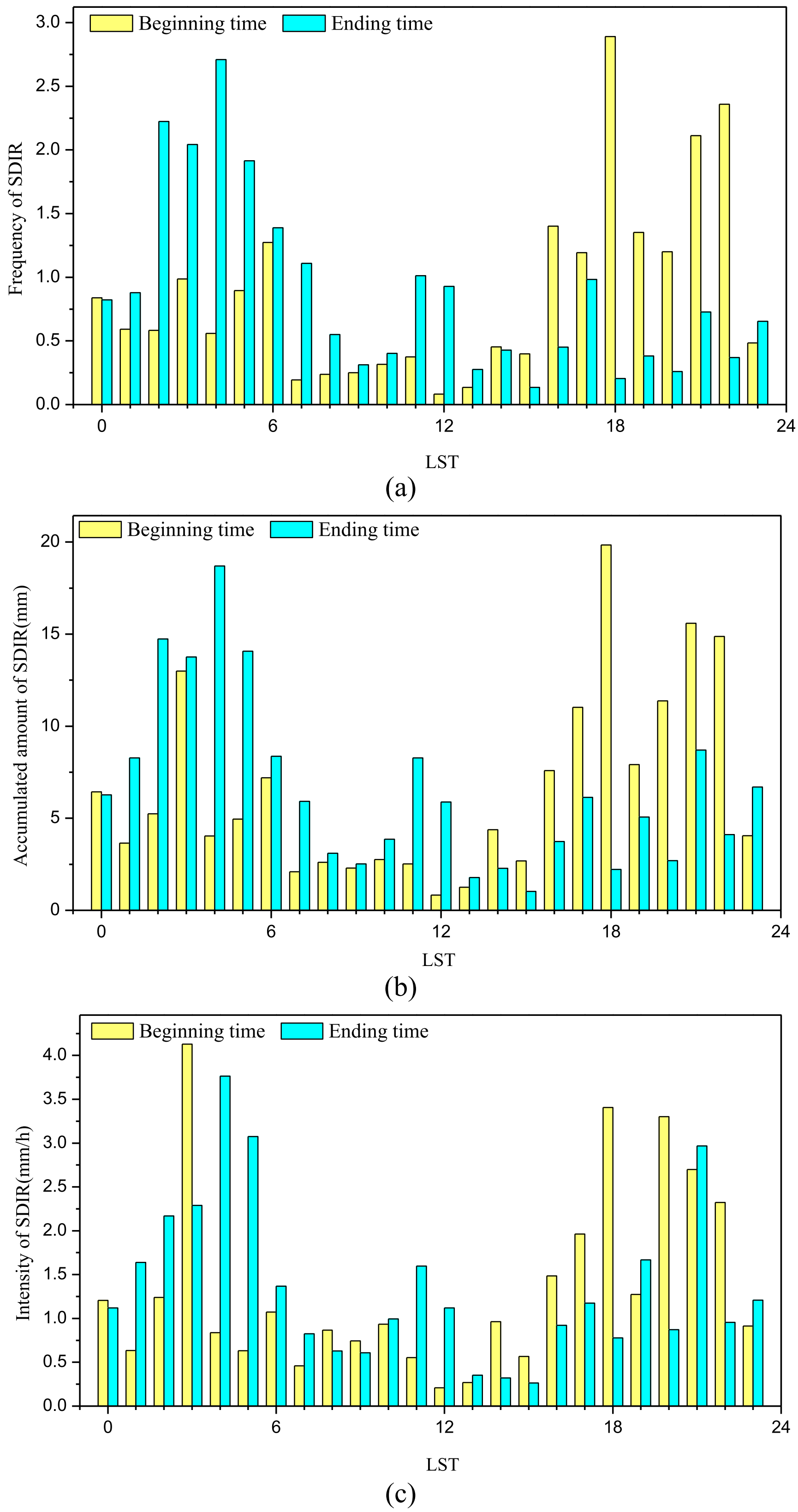

FIG. 5. Diurnal variations of (a) frequency, (b) amount, and (c) intensity of SDIR events with different beginning (yellow) and ending times (cyan) in the urban areas of Beijing Municipality.

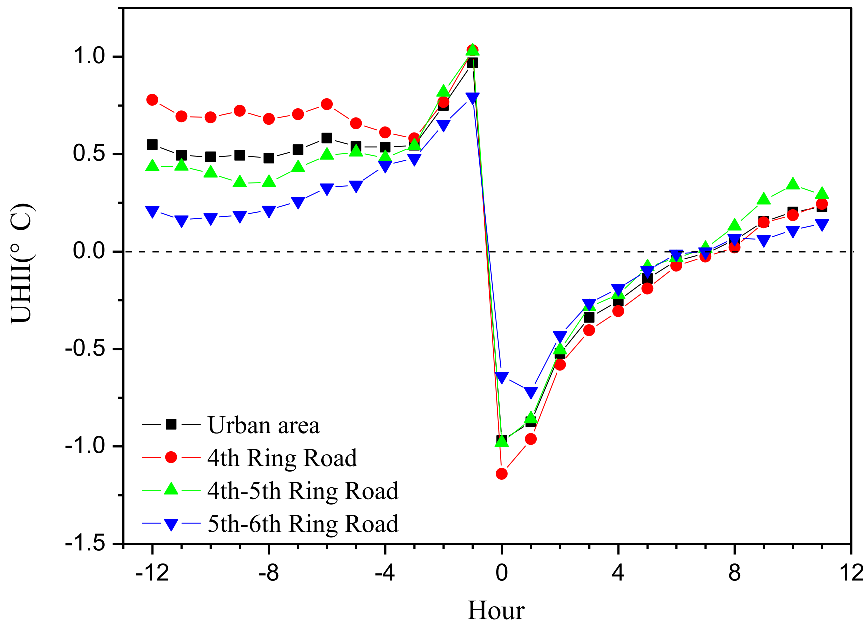

(a)

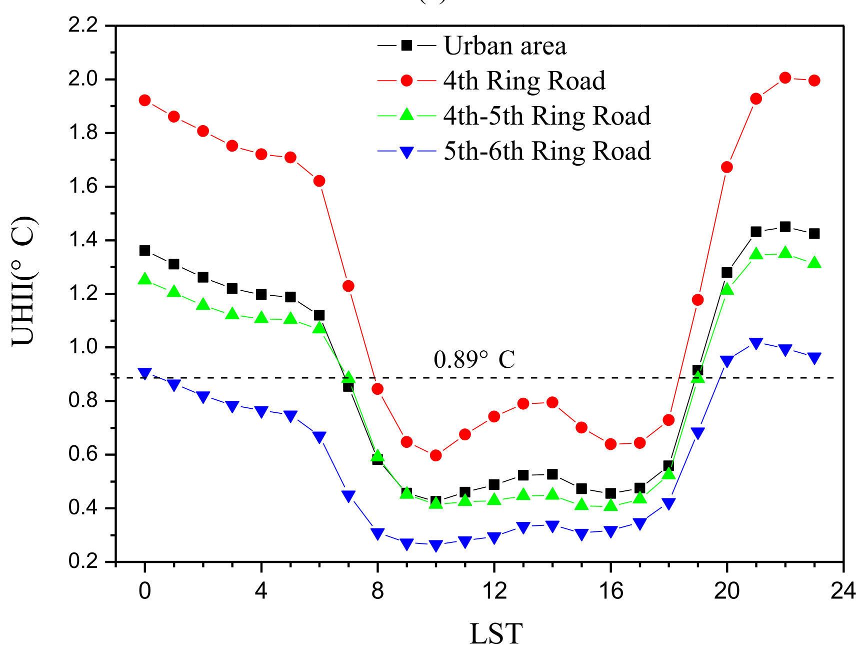

(b)

FIG. 6. (a) Variation of UHII before and after the beginning time of SDIR events for different urban areas (level dotted line denotes UHII of 0°C), and (b) the diurnal variation of UHII in summer for different urban areas (level dotted line denotes the daily mean UHII of 0.89°C). Different urban areas include the entire urban area (inside the Sixth RR) and the 4th, 4th–5th, and 5th–6th RR areas.

The swift drop of the UHII at the moment of the appearance of the SDIR events could be explained by the cooling effect of the intense rainfall in the urban areas, sometimes characterized by downpours or even downbursts with strong dragging flows downward to the ground surface, effectively decreasing the surface air temperature at the sites where the SDIRs occur. Since the SDIR events mostly occur in urban areas, the surface air temperature at the rural stations may remain relatively higher, and the differences of temperature between the urban and rural areas become negative values. After the beginning of the SDIR events, the UHII remains negative due to the continuous rainfall and the wet ground surface, but recovers gradually and becomes positive once again at about +6 to +8 h. Therefore, a cool island phenomenon, and probably a cool island circulation, has been formed during the SDIR event occurrence with the strongest cooling seen at the beginning hour of the SDIR events.

There are some differences of UHII variation before and after the beginning time of SDIR events for the three summer months (Fig. 7a). In general, the variations of UHII of the different months are similar. Before the SDIR beginning time, the UHII is positive and around 0.5°C, and after that, the UHII bottoms out at the zero time and then picks up quickly in four hours and increases slowly to around 0°C. The features of UHII variation in August are somewhat different from those in June and July because it is always higher before the beginning time of SDIR events and lower after that. It is also interesting to note that the rapid rise of the UHII occurs one hour earlier between −3 and −2 h for the August SDIR events.

Figure 7b shows the differences of the UHII before and after the beginning time of the SDIR events during different diurnal periods based on the UHII variation as described in Yang et al. (2013b). The disparities of the UHII variations in different diurnal periods are apparent. During the relatively stable high UHII stage (2100–0500 LST), the highest UHII (1.2°C) is reached at one hour ahead of the zero time, and it bottoms out an hour after the beginning time. Another phenomenon during this stage is that the UHII climbs slowly and remains below 0°C for a longer period after the zero time. For the relatively stable low UHII stage (1100–1500 LST), the highest UHII occurs far from the zero time between −12 and −8 h, rather than at −1 or −2 h as usually seen. The lowest UHII, −1.8°C, appears at about one hour after the beginning time of the SDIR events during the relatively stable low UHII stage.

Figure 8 shows spatial distribution of the UHII at typical moments before and after the beginning of the SDIR events. The discrepancy of the UHII spatial distribution is obvious. The UHII distributions at 6 and 3 h before the beginning of the SDIR events exhibit high-value centers in the urban areas. The stations farther away from urban center usually have lower UHII values. This spatial pattern is approximately line with the distribution of the SDIR events. The UHII one hour before the beginning of the SDIR events has the highest values within the studied period. Except for the northeast, the whole studied area is characterized by high UHII, with the highest value center of more than 1.6°C in the west of urban center. When the SDIR events begin to occur, however, the UHII of each station over the whole studied area suddenly drops to negative values (Fig. 8d), with the lowest UHII value in Hai Dian (HD), northwest of the urban center. The pattern of the UHII at the beginning of the SDIR events indicates the largest temperature drop in the northwest of the urban areas caused by the more frequent or more intense SDIR events, as shown in Fig. 2. The pattern can also be seen for the moments of +1 and +3 h. After the beginning of the SDIR events, however, the UHII gradually increases, and it partially rises to positive values at about +6 h. Certainly, the spatial distributions of the UHII after zero time have no distinct connection with the spatial patterns of the SDIR events.

Figure 9 shows the spatial correlation coefficients of the UHII of different hours before and after the zero time with the SDIR frequency and rainfall amount at all the stations of the urban areas. The variation of spatial correlation coefficients of UHII with SDIR frequency is similar to that with SDIR amount. The correlation coefficients at 5 h or more before the zero time are all significant at the 99% confidence level, and those at 4 and 3 h before the zero time are significant at the 95% confidence level. There is no notable correlation at −2 and −1 h. It is therefore evident that, although the UHII at −1 or −2 h is more indicative of the beginning of the SDIR events, the occurrence of the SDIR events depends more on the magnitude of the UHII over 3 h ago, and especially over 5 h ago. It may be probably explained by the fact that any SDIR event related to the UHI effect needs time to generate and develop.

After the SDIR events begin, the UHII correlations with the SDIR event frequency and rainfall amount become negative, with the negative values being the largest at the beginning hour and gradually going back to positive correlations after about +5 h. However, all the negative correlations do not pass the significance test. The negative correlations should be a reflection of the influence of SDIR events on the UHII at the stations.

c. *Regional SDIR events*

Extremely intense weather events usually occur at the approximately same time within a given region (Li and Chou 1990; Li and Zhang 2009; Li et al. 2010; Yang et al. 2012, 2013c). This phenomenon can be regarded as regional or clustering extreme events. According to the definition of regional SDIR as given above, we examine the main features of the regional SDIR events in the urban area inside Sixth RR using the 8-yr data collected from the urban stations.

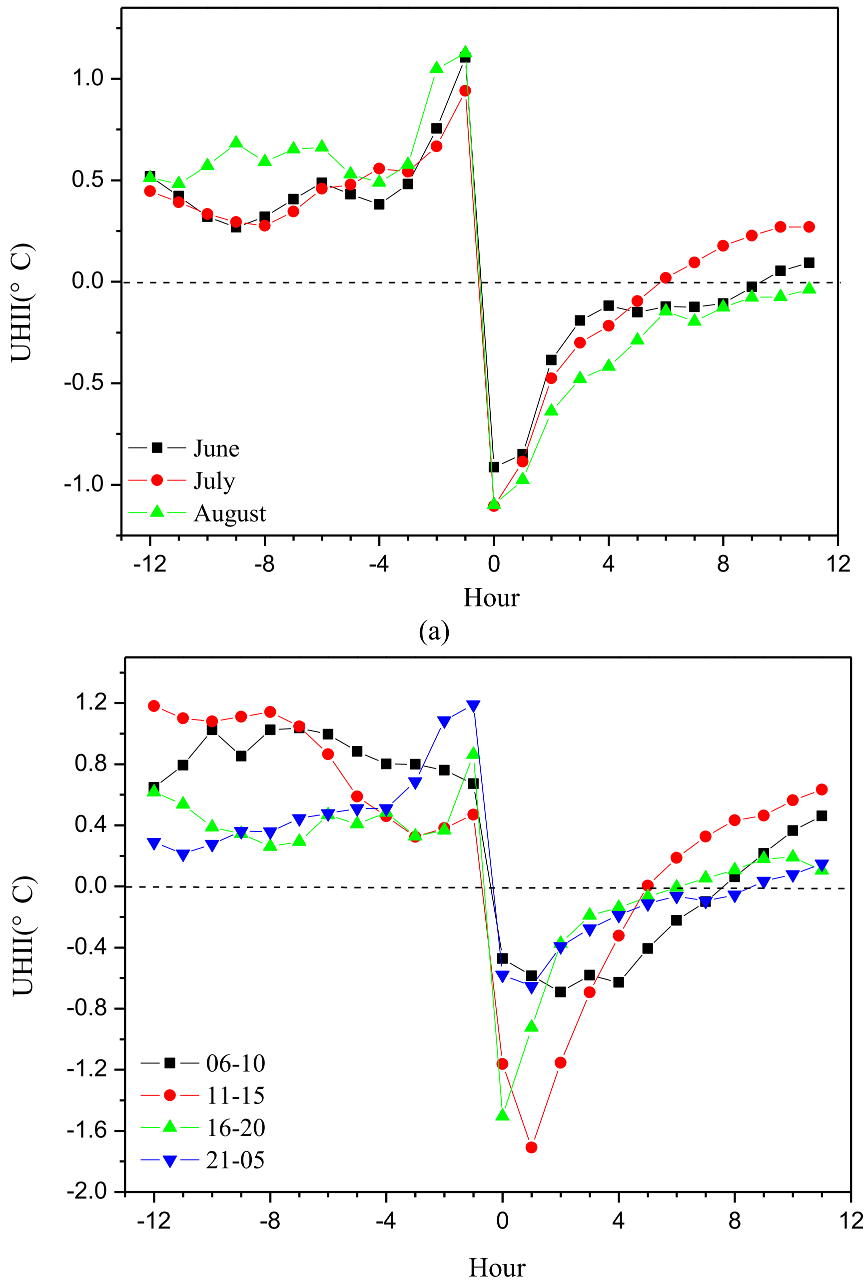

FIG. 7. (a) UHII variation before and after the beginning time (horizontal line is 0°C) of SDIR events for summer months (black, red, and green dotted lines denote June, July, and August respectively), and (b) typical diurnal periods of UHII (black, red, green, and blue dotted lines denote 6–10 h (rapidly declining period), 11–15 h (stable period with weak UHII), 16–20 h (rapidly increasing period) and 21–05 h (stable period with strong UHII) respectively).

In the period 2007–14, 38 regional SDIR events are identified in the urban areas. Figure 10a shows that, whenever the earliest (beginning) or the latest (end) occurrence time, the regional SDIR events tend to take place more frequently in the period 1800–2200 LST. There is no regional SDIR event that begins during 0800–1300 LST. The diurnal variation of the beginning and end time of the regional SDIR events seem to be similar to that of the UHII, with a relatively stable high-frequency period of 1800–2200 LST and a relatively

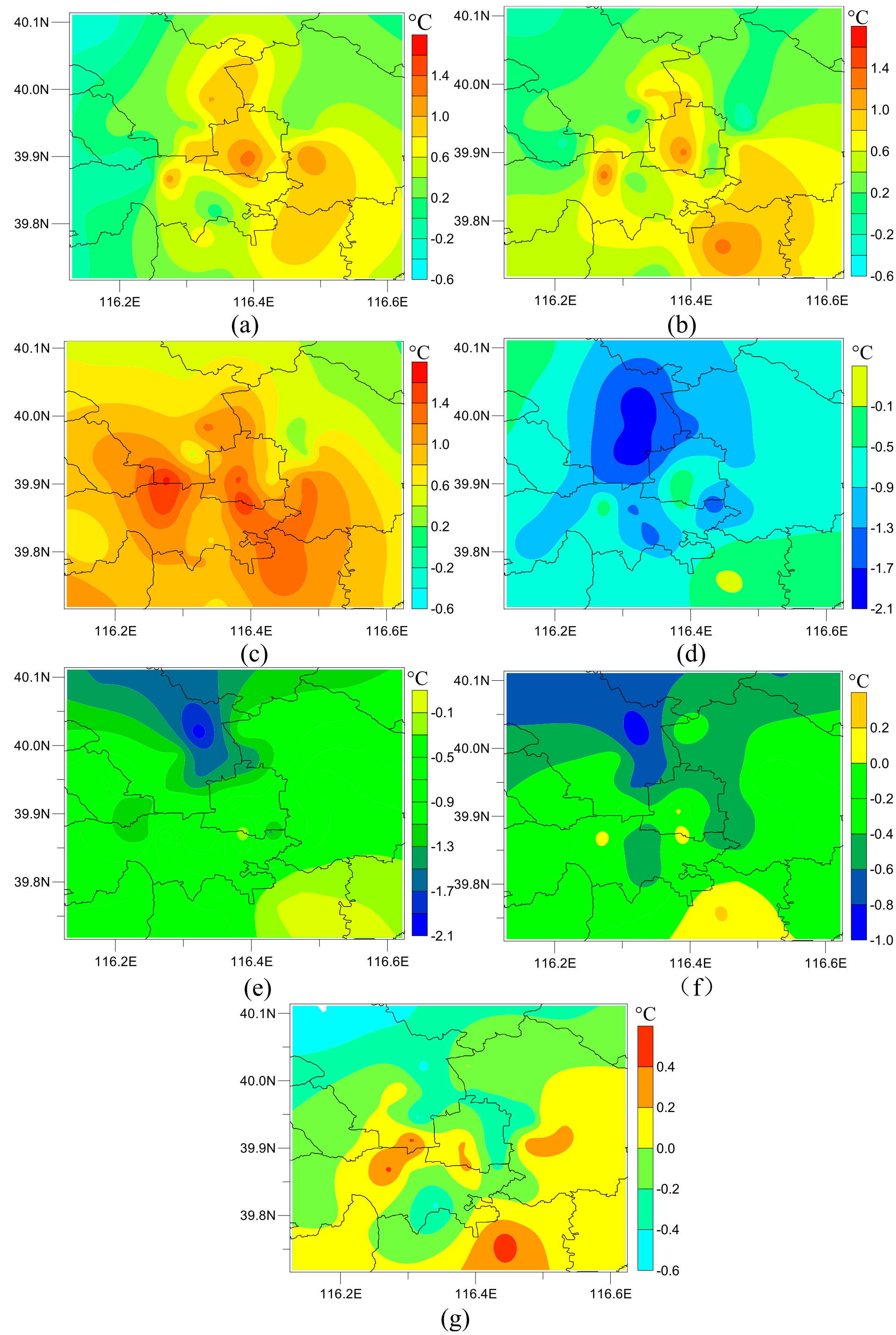

FIG. 8. Spatial distribution of UHII in urban area of Beijing at typical moments before and after the beginning time of the SDIR events within 24 h for (a)–(c) 6, 3, and 1 h before the SDIR and (e)–(g) 1, 3, and 6 h after the SDIR, and (d) at 0 h (SDIR).

stable low-frequency period of 0800–1300 LST. Comparing the diurnal variations of the UHII and the beginning and end time of the regional SDIR events, however, it is found that the relatively stable low-frequency period (0800–1300 LST) of the beginning and end time of the regional SDIR events corresponds to the swiftly decreasing stages (0600–1000 LST) of the UHII but lags about 2 h later. Similarly, the relatively

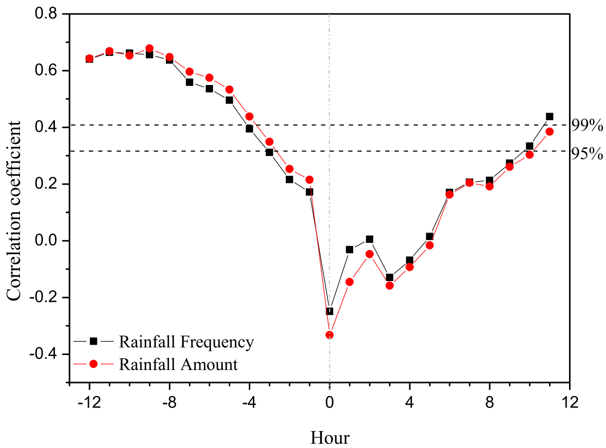

FIG. 9. The spatial correlation coefficients of the UHII of various hours before and after the beginning time of frequency and rainfall amount of SDIR events at all the stations in the urban areas. Two level dotted lines denote that the correlation coefficients are significant at 95% and 99% confidence level, respectively.

stable high-frequency period (1800–2200 LST) of the beginning and end time of the regional SDIR events lags behind the swiftly ascending stages (1600–2000 LST) of the UHII by about 2 h. It seems that, when the UHII drops swiftly, the regional SDIR events will take place more rarely, and when the UHII surges, the regional SDIR events will occur more frequently.

The beginning and end times of the regional SDIR events demonstrate a clearer diurnal cycle than that of the site-based SDIR events. The diurnal variation pattern provides stronger evidence that the UHII and its variation might have affected the formation and development of the regional SDIR events in the urban areas of Beijing. The low- and high-frequency periods of the beginning and end times of the regional SDIR events generally lag behind the rapidly declining and rising stages of the UHII, which might be an indication that the regional SDIR events need time to respond to the change of the thermal condition of the underlying surface.

Figure 10b shows the spatial distribution of the total numbers of the regional SDIR events as recorded for each station during 2007–14. It is clear that the high-value center is located in the urban center of Beijing. The stations Si Hui Qiao (located in the eastern part of the urban center) and Da Guan Yuan (in the southwest part of urban center) have the greatest frequencies of regional SDIR of 17 times during the 8-yr period. Both of them are located inside the Fourth RR. Most of other stations with high values are located inside the Fifth RR. The sites farthest away from the urban center, such as Dao Xiang Hu (the site labeled 4 in Fig. 10b) and Hou Sha Yu (labeled 6 in Fig. 10b), see the lowest frequencies of the regional SDIR events.

Figure 11 shows the urban area averaged UHII before and after the occurrence of the regional SDIR events in a day. The UHII at 1 h before the beginning time of the regional SDIR events reaches the highest level, and it then drops quickly to the lowest level at about 1–2 h after the beginning time of the regional SDIR events. From 1 to 4 h after the beginning time of the regional SDIR events, however, the UHIIs are apparently lower than zero. These features are generally similar to the annual mean UHII variation for the site-based SDIR events (Figs. 6 and 7). The difference is that the UHII in case of the site-based SDIR events is negative at the beginning time, while the UHII with the regional SDIR events is still apparently greater than zero at the beginning time. This is because the beginning time of a regional SDIR event is defined as the first hour of all the beginning hours of the stations experiencing the event, and the average beginning time of the site-based SDIR events is later than that.

We also calculate the diurnal variation of various meteorological variables of a representative station BO before and after the beginning of the regional SDIR events (Figs. 12a–d). About four hours before the regional SDIR events, the surface air temperature of BO remains relatively steady at about 28°C. Then the temperature begins to drop remarkably to about 26.5°C at zero time, about 22°C around +7 h and after. The diurnal variation of temperature may reflect a combined effect of normal diurnal temperature cycle and the interaction of the UHII and the regional SDIR events. As the high-frequency periods of the beginning and end times of the regional SDIR events appear between 1800 and 2200 LST, the highest temperature between −8 and −4 h in Fig. 12a equivalently occurs from 1200 to 1600 LST. However, the variation of the UHII before and after the beginning of the regional SDIR events may have modified the natural diurnal temperature cycle.

Figure 12b shows variations of surface air pressure before and after the beginning of the regional SDIR events. It is obvious that the pressure keeps a sustained downward trend from about 12 to 1 h before the zero time. The lowest level is reached at about −1 h, and then it begins to rapidly increase and arrive at the peak in about 6 h. Although the pressure diurnal variation may have been partly controlled by the natural diurnal cycle, its unnatural plunging from about −7 to −1 h and the violent rising after the beginning of the regional SDIR events may represent a response to the variation of the UHI circulation and the locally generated intense mesoscale system.

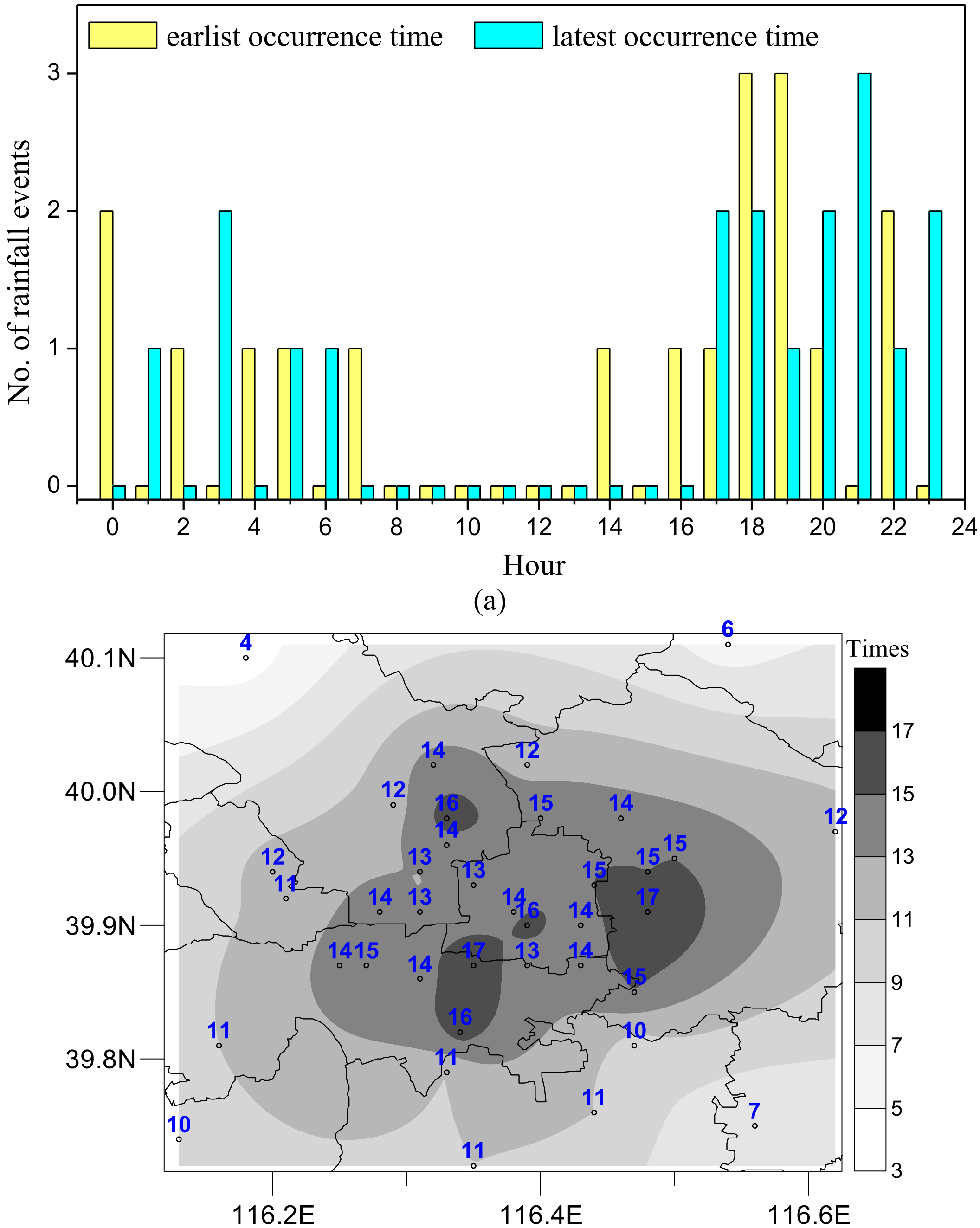

(a)

(b)

FIG. 10. (a) Numbers of regional SDIR events with the earliest (yellow) and latest (cyan) occurrence time in a day, and (b) the spatial distribution of the total numbers of the regional SDIR events as recorded for each station (denoted by isograms; number of events for each stationshown in blue), during 2007–14.

The variation of relative humidity (Fig. 12c) is almost opposite to that of the temperature curve (Fig. 12a). Before the regional SDIR event begins, the relative humidity exhibits a small magnitude fluctuation with the lowest values of about 70% appearing from −8 to −6 h. At about −4 or −3 h, it begins to increase rapidly until 4 to 6 hours after the beginning time of the regional SDIR when it peaks at about 92%. Even at the lowest values, the relative humidity is still well above 68%, indicating that the sufficient near-surface atmospheric moisture is a precondition for the regional SDIR events to develop. The high relative humidity after the beginning

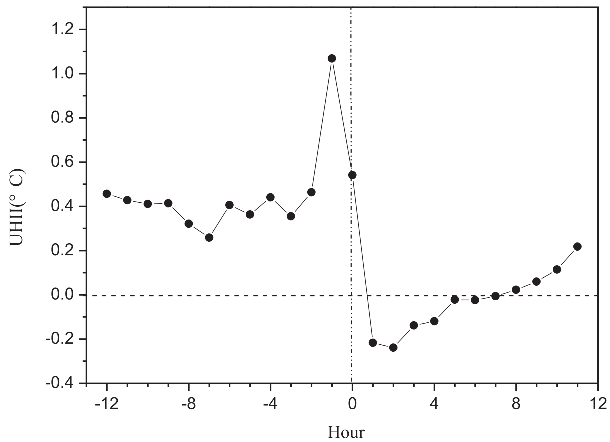

FIG. 11. The urban area averaged UHII before and after the beginning time of the regional SDIR events within 24 h; the level dotted line denotes UHII of 0°C.

of the regional SDIR events is obviously related to the rainfall.

Figure 12d shows the pattern of wind speed and direction of the BO accompanying the regional SDIR events. The dominant near-surface airflow is in the southeast direction before the beginning time of the regional SDIR events, and in the northeast direction after. At about −3 to −1 h, the flow is mainly from the east, with the wind speed at −1 h reaching the largest values for the period before the arrival of the SDIR events. This change in wind direction and speed can be attributed to the interaction between the UHI circulation and the synoptic system passing over the station during the SDIR events, with the BO wind direction experiencing a clockwise rotation.

4. Discussion

In previous research, it was found that the strongest UHII generally appeared within or around the Fourth RR in Beijing City, in accordance with Beijing's major transportation system with a multiple ring road network (Yang et al. 2013b). It was also demonstrated that short-duration heavy rainfall events dominate summer rainfall in urban regions of Beijing (Yang et al. 2013a). However, the previous works are separate and unassociated with each other. In fact, there are some meaningful numerical analyses that have simulated the impacts of urbanization on urban climates and the results indicate that urbanization has the potential to increase precipitation especially in summer (Zhang et al. 2010; Miao et al. 2011; Zhan et al. 2013). It is necessary and imperative to find more observational evidences for the possible relations between urbanization and precipitation. The analysis presented in the study focuses on

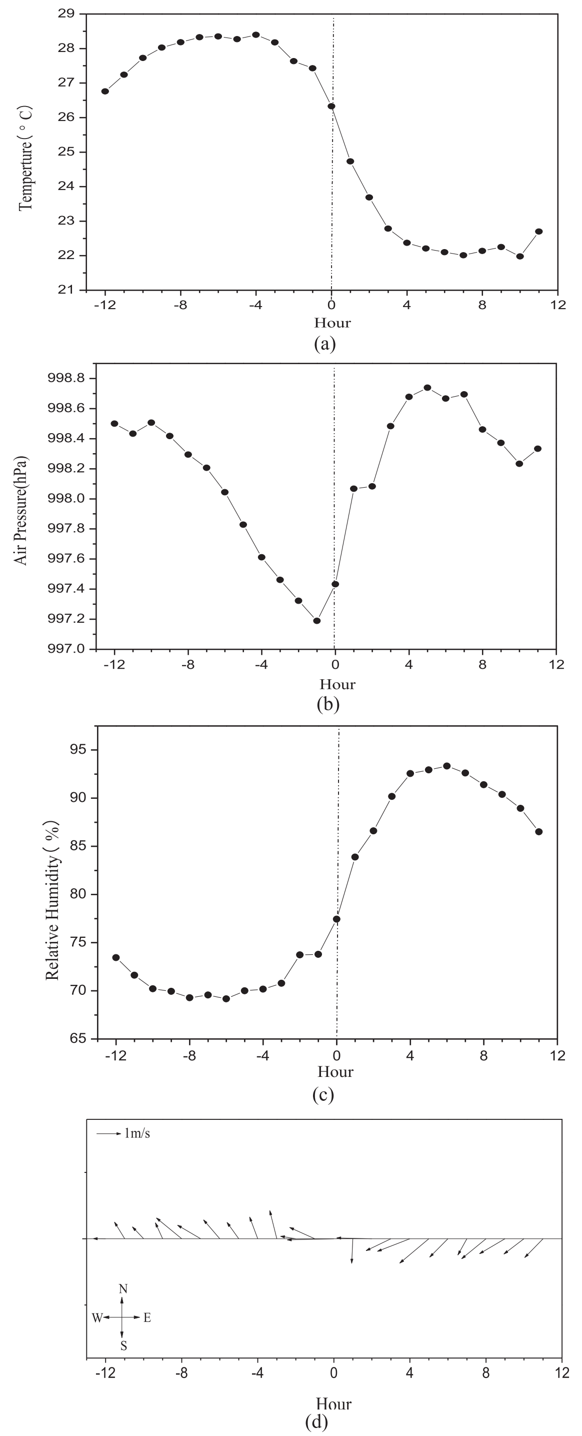

FIG. 12. Diurnal variation of (a) surface air temperature, (b) surface air pressure, (c) relative humidity, and (d) wind speed and direction at Beijing Observation (BO) before and after the beginning time of the regional SDIR events. All of the vertical lines in (a)–(c) denote beginning time of regional SDIR events.

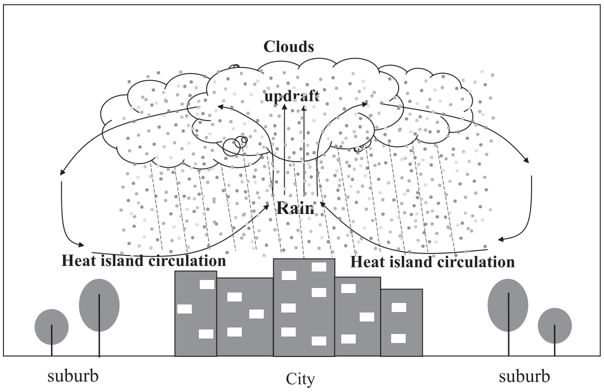

FIG. 13. A sketch of urban thermal effects on precipitation.

both site-based and regional SDIR events. The possible relationships between the UHII and the SDIR events are examined. Interestingly, evidence for a strong association of SDIR events with urbanization has been found in the study.

First, for both the site-based and the regional SDIR events, their spatial patterns are approximately in accordance with the magnitude of urbanization, including density of population and buildings and transportation intensity (see Figs. 2 and 10b). High-intensity anthropogenic activity areas are also characterized by the strongest UHII, indicating a spatial correspondence between the SDIR events and the UHII. Second, for both site-based SDIR events and regional SDIR events, the diurnal variations of the UHII before and after the beginning time of the SDIR events are both separated into two different periods by beginning time (see Figs. 6a and 11), showing a strong temporal association between SDIR events and UHII. The phenomenon of the strong association of SDIR events with the UHI effect is easily understandable, and it can be elaborated by the sketch of precipitation formation in the city (Fig. 13). Urbanization leads to a highly urbanized underlying surface, increasing anthropogenic heat release, and a greater presence of aerosols, which have changed the radiation budget in the urban canopy and urban boundary layer. All of the above reasons explain why urban areas remain persistently warmer than their surroundings, and the ambient field is changed and eventually forms UHI circulation. Many observational studies and numerical simulations confirm that UHI circulation exists under certain weather conditions (e.g., Angell et al. 1973; Auer 1974; Li and Chou 1990). The UHI circulation triggers water vapor transport and convergence upward movement. Thus, if there is enough moisture in the air, more intense rainfall events could easily occur in the urban areas.

In terms of diurnal variations, a very good correspondence between the UHII and frequency and rainfall amount of the SDIR events over the urban areas of Beijing has been found, as shown in Figs. 5, 6, 7, and 10. The SDIR events generally begin in the evening and end in the late night and early morning, with the daytime seeing the least occurrence. The diurnal variation is consistent with that of the UHII as previously reported by Yang et al. (2013b). This is because the strengthened UHII causes an increased magnitude of UHI circulation in the urban areas after the sunset, with the uplift branch in the central area near or within the Fourth RR, increasing the possibility for the SDIR events to occur during late evening and the nighttime. With the weakening of the UHII during morning and noontime, the air convection in the central urban area also becomes less remarkable, and the frequencies of the SDIR events will be lower. The mountain–valley breeze circulation between the urban areas and the mountains of the west and north (Liu et al. 2014) may superpose over the UHI circulation, and may further strengthen the convection movement in the central urban area.

Aerosols in urban areas may have a more complicated influence, but they may also promote to a certain extent the formation of the SDIR events in case of sufficient moisture during midsummer (Rosenfeld et al. 2008). There has been much study about how aerosols affect urban precipitation. Some studies have demonstrated that cities with heavy pollution probably generate more intense rainfall events (Shepherd and Burian 2003; Guo et al. 2014), while some other works have drawn the opposite conclusion that aerosols decrease or restrain precipitation (e.g., Rosenfeld 1999, 2000; Givati and Rosenfeld 2004). It is possible that the effect of aerosols on urban precipitation is seasonal and site dependent, with the positive effect or rain-enhancing role occurring chiefly in moist tropical cities and rainy seasons of monsoon-zone cities. In our previous research (Yang et al. 2017) and in this study, we found that urban areas with heavier pollution experience more frequent SDIR events. Chen et al. (2015) also found that the urban areas of the Pearl River Delta in southern China have less frequent and shorter-duration rain events and larger hourly mean rainfall in the afternoon, compared to the surrounding rural areas. This might be caused by the stronger convection due to the UHI effect and the stagnating effect of synoptic systems due to the increased surface roughness, but might also relate to the higher concentration of aerosols in the urban boundary layer. An opposite result was reported by Kaufmann et al. (2007), however, showing a reduction in rainfall during the dry winter monsoon season over the urban areas of the Pearl River Delta. Therefore, sufficient water vapor might be a prerequisite for realization of the aerosol positive effect in promoting urban precipitation,

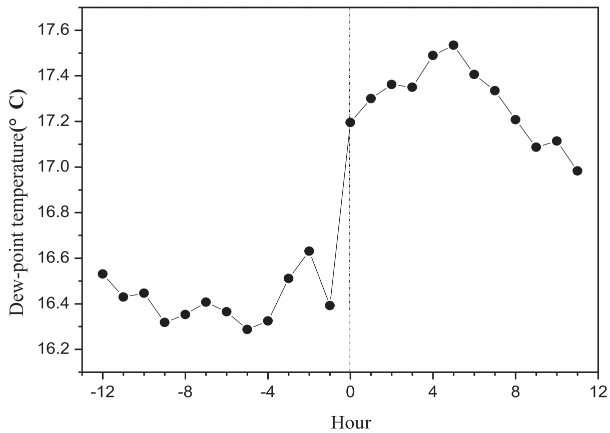

FIG. 14. The urban area averaged dewpoint temperature before and after the beginning time of the SDIR events within 24 h. The level dotted line denotes UHII of 0°C.

but obviously this issue still needs more research in the future.

Water vapor is an important element for forming the urban SDIR events regardless of existence of aerosols. In addition to analyzing the relation of relative humidity and SDIR (Fig. 12c), which shows the influence of water vapor on formation and development of the SDIR events, dewpoint temperature variation of urban area before and after the beginning time of the SDIR events within 24 h is examined here and the result is shown in Fig. 14. It can be seen that the dewpoint temperatures maintain low values before the beginning time, whereas the values remain relatively high after the beginning time. Interestingly, the dewpoint temperature experiences a slight rise from 4 to 2 h before the beginning time of the SDIR events, indicating that the increasing water vapor may indeed play a role in generating the SDIR, and the prophase anomalies of both relative humidity and dewpoint temperature could also be taken as indicators of the generation and development of SDIR events.

5. Conclusions

This paper examines the climatological characteristics of the short-duration intense rainfall (SDIR) events in Beijing urban areas, and the relationships between the UHI intensity and the SDIR events by using the hourly data collected from a high-density automatic weather station (AWS) network. The following conclusions are drawn from the analysis:

1) The annual mean frequency (amount) of the SDIR events over the urban areas is 3.2 events (158.2 mm), obviously larger than those over the rural areas, and the highest annual mean frequency and rainfall amount all occur in or near the central urban area. The highest values of frequency, amount, and intensity of the SDIR events are all in the last 10-day period in July, with the large values occuring in summer and no SDIR events in winter.
2) Most of the SDIR events begin to occur in late evening and early night from 1600 to 2200 LST and late night from 0000 to 0600 LST. The lowest SDIR events are observed to begin from 1200 to 1300 LST. The SDIR events generally tend to end in late night and early morning from 0200 to 0700 LST.
3) The UHII in urban areas maintains high values before the beginning of the SDIR events, but stays low or even becomes negative after that. The highest UHII appears in the hour before the beginning of the SDIR events, and then it swiftly falls to a large negative value when the SDIR events begin. The UHII variation is regarded as both a driver of the convection and the SDIR development and a result of the SDIR events.
4) Correlation coefficients of the UHII with the SDIR frequency (amount) are all highly significant for over 3 h before the beginning of the SDIR events. Although the UHII at immediate hours before the SDIR appearance is more indicative of the beginning of the SDIR events, their occurrence more depends on the magnitude of the UHII more than 3 h ahead.
5) The UHII before the beginning of the SDIR events exhibit high-value centers in the central urban areas. The spatial pattern is generally line with the distribution of the SDIR events. When the SDIR events begin to occur, however, the UHII of each station over the urban areas suddenly drops to negative values.
6) The spatial and temporal patterns of regional SDIR events exhibit similar characteristics of the site-based SDIR events, and also show a good relationship with the UHII in the urban areas, indicating the possible influence of the urban factor on the SDIR formation and development, and the impact of the SDIR events on the UHII.
7) In addition to the UHII of the urban areas, surface air temperature, surface air pressure, relative humidity, and near-surface wind directions at the Beijing Observatory also exhibit large changes before and after the beginning of the regional SDIR events, and have potential to indicate the occurrence of the SDIR events in the studied area.

Acknowledgments. This study is financially supported by the China Natural Science Foundation (CNSF) (Grants 41375069, 41575003, and 41675092) and the Ministry of Science and Technology of China (Grant GYHY201206012).

REFERENCES

Allen, M. R., and W. J. Ingram, 2002: Constraints on future changes in climate and the hydrologic cycle. *Nature*, **419**, 224–232, doi:10.1038/nature01092.

Angell, J. K., W. H. Hoecker, H. P. Dickson, and D. H. Pack, 1973: Urban influence on strong daytime air flow as determined from tetroon flights. *J. Appl. Meteor.*, **12**, 924–936, doi:10.1175/1520-0450(1973)012<0924:UIOASD>2.0.CO;2.

Arnfield, A. J., 2003: Two decades of urban climate research: A review of turbulence, exchanges of energy and water, and the urban heat island. *Int. J. Climatol.*, **23**, 1–26, doi:10.1002/joc.859.

Auer, A. H., 1974: Cumulus congestus growth downwind in St. Louis, Missouri: Case study. *J. Wea. Modif.*, **6**, 229–237.

Bornstein, R. D., and G. M. LeRoy, 1990: Urban barrier effects on convective and frontal thunderstorms. *Extended Abstracts, Fourth Conf. on Mesoscale Processes*, Boulder, CO, Amer. Meteor. Soc., 120–121.

Changnon, S. A., 1968: The La Porte weather anomaly—Fact or fiction? *Bull. Amer. Meteor. Soc.*, **49**, 4–11.

——, 1979: Rainfall changes in summer caused by St. Louis. *Science*, **205**, 402–404, doi:10.1126/science.205.4404.402.

——, R. T. Shealy, and R. W. Scott, 1991: Precipitation changes in fall, winter, and spring caused by St. Louis. *J. Appl. Meteor.*, **30**, 126–134, doi:10.1175/1520-0450(1991)030<0126:PCIFWA>2.0.CO;2.

Chen, S., W.-B. Li, Y.-D. Du, C.-Y. Mao, and L. Zhang, 2015: Urbanization effect on precipitation over the Pearl River Delta based on CMORPH data. *Adv. Climate Change Res.*, **6**, 16–22, doi:10.1016/j.accre.2015.08.002.

Craig, K. J., and R. D. Bornstein, 2002: MM5 simulations of urban induced convective precipitation over Atlanta. *Fourth Symp. on the Urban Environment*, Norfolk, VA, Amer. Meteor. Soc., 1.3. [Available online at https://ams.confex.com/ams/AFMAPUE/techprogram/paper_38803.htm.]

Diem, J. E., and D. P. Brown, 2004: Anthropogenic impacts on summer precipitation in central Arizona, U.S.A. *Prof. Geogr.*, **55**, 343–355.

Dou, J., Y. Wang, R. Bornstein, and S. Miao, 2015: Observed spatial characteristics of Beijing urban climate impacts on summer thunderstorms. *J. Appl. Meteor. Climatol.*, **54**, 94–104, doi:10.1175/JAMC-D-13-0355.1.

Givati, A., and D. Rosenfeld, 2004: Quantifying precipitation suppression due to air pollution. *J. Appl. Meteor.*, **43**, 1038–1056, doi:10.1175/1520-0450(2004)043<1038:QPSDTA>2.0.CO;2.

Guo, X., D. Fu, X. Guo, and C. Zhang, 2014: A case study of aerosol impacts on summer convective clouds and precipitation over northern China. *Atmos. Res.*, **142**, 142–157, doi:10.1016/j.atmosres.2013.10.006.

Han, J.-Y., and J.-J. Baik, 2008: A theoretical and numerical study of urban heat island–induced circulation and convection. *J. Atmos. Sci.*, **65**, 1859–1877, doi:10.1175/2007JAS2326.1.

——, ——, and H. Lee, 2014: Urban impacts on precipitation. *Asia-Pac. J. Atmos. Sci.*, **50**, 17–30.

Hennessy, K. J., J. M. Gregory, and J. F. B. Mitchell, 1997: Changes in daily precipitation under enhanced greenhouse conditions. *Climate Dyn.*, **13**, 667–680, doi:10.1007/s003820050189.

Huff, F. A., 1986: Urban hydrometeorology review. *Bull. Amer. Meteor. Soc.*, **67**, 703–711.

Jáuregui, E., 1973: The urban climate of Mexico City. *Erdkunde*, **27**, 298–307, doi:10.3112/erdkunde.1973.04.06.

Kalnay, E., and M. Cai, 2003: Impact of urbanization and land-use change on climate. *Nature*, **423**, 528–531, doi:10.1038/nature01675.

Kaufmann, R. K., K. C. Seto, A. Schneider, Z. Liu, L. Zhou, and W. Wang, 2007: Climate response to rapid urban growth: Evidence of a human-induced precipitation deficit. *J. Climate*, **20**, 2299–2306, doi:10.1175/JCLI4109.1.

Kishtawal, C. M., D. Niyogi, M. Tewari, R. A. Pielke Sr., and J. M. Shepherd, 2010: Urbanization signature in the observed heavy rainfall climatology over India. *Int. J. Climatol.*, **30**, 1908–1916, doi:10.1002/joc.2044.

Li, J., and L. Zhang, 2009: Wind onset and withdrawal of Asian summer monsoon and their simulated performance in AMIP models. *Climate Dyn.*, **32**, 935–968, doi:10.1007/s00382-008-0465-8.

——, R. Yu, and J. Wang, 2008: Diurnal variations of summer precipitation in Beijing. *Chin. Sci. Bull.*, **53**, 1933–1936.

——, Z. Wu, Z. Jiang, and J. He, 2010: Can global warming strengthen the East Asian summer monsoon? *J. Climate*, **23**, 6696–6705, doi:10.1175/2010JCLI3434.1.

Li, W., and J. Chou, 1990: The relative characteristics of time and space of monthly mean precipitation over China. *Plateau Meteor.*, **9**, 284–292.

Liang, P., Y. H. Ding, J. H. He, and X. Tang, 2013: Study of relationship between urbanization speed and change of spatial distribution of rainfall over Shanghai. *J. Trop. Meteor.*, **19**, 97–103.

Lin, C.-Y., W.-C. Chen, P.-L. Chang, and Y.-F. Sheng, 2011: Impact of the urban heat island effect on precipitation over a complex geographic environment in northern Taiwan. *J. Appl. Meteor. Climatol.*, **50**, 339–353, doi:10.1175/2010JAMC2504.1.

Lin, Y. L., and R. B. Smith, 1986: Transient dynamics of airflow near a local heat source. *J. Atmos. Sci.*, **43**, 40–49, doi:10.1175/1520-0469(1986)043<0040:TDOANA>2.0.CO;2.

Liu, W., H. You, G. Ren, P. Yang, and B. Zhang, 2014: AWS precipitation characteristics based on *k*-means clustering method in Beijing area. *Meteor. Mon.*, **10**, 844–851.

Miao, S., F. Chen, Q. Li, and S. Fan, 2011: Impacts of urban processes and urbanization on summer precipitation: A case study of heavy rainfall in Beijing on 1 August 2006. *J. Appl. Meteor. Climatol.*, **50**, 806–825, doi:10.1175/2010JAMC2513.1.

Mishra, V., J. M. Wallace, and D. P. Lettenmaier, 2012: Relationship between hourly extreme precipitation and local air temperature in United States. *Geophys. Res. Lett.*, **39**, L14603, doi:10.1029/2012GL052790.

Mölders, N., and M. A. Olson, 2004: Impact of urban effects on precipitation in high latitudes. *J. Hydrometeor.*, **5**, 409–429, doi:10.1175/1525-7541(2004)005<0409:IOUEOP>2.0.CO;2.

Ochoa, C. A., A. I. Quintanar, G. B. Raga, and D. Baumgardner, 2015: Changes in intense precipitation events in Mexico City. *J. Hydrometeor.*, **16**, 1804–1820, doi:10.1175/JHM-D-14-0081.1.

Oke, T. R., 1976: The distinction between canopy and boundary-layer urban heat islands. *Atmosphere*, **14**, 269–277.

——, 1982: The energetic basis of the urban heat island. *Quart. J. Roy. Meteor. Soc.*, **108**, 1–24, doi:10.1002/qj.49710845502.

——, 1987: *Boundary Layer Climates*. Methuen and Co., 435 pp.

——, 1988: The urban energy balance. *Prog. Phys. Geogr.*, **12**, 471–508, doi:10.1177/030913338801200401.

Pathirana, A., H. B. Denekew, W. Veerbeek, C. Zevenbergen, and T. A. Banda, 2014: Impact of urban growth-driven land use change on microclimate and extreme precipitation—A sensitivity study. *Atmos. Res.*, **138**, 59–72, doi:10.1016/j.atmosres.2013.10.005.

Ren, G., and Y. Zhou, 2014: Urbanization effects on trends of extreme temperature indices of national stations over mainland China, 1961–2008. *J. Climate*, **27**, 2340–2360, doi:10.1175/JCLI-D-13-00393.1.

——, ——, Z. Chu, J. Zhou, A. Zhang, J. Guo, and X. Liu, 2008: Urbanization effects on observed surface air temperature trends in north China. *J. Climate*, **21**, 1333–1348, doi:10.1175/2007JCLI1348.1.

Ren, Y., and G. Ren, 2011: A remote-sensing method of selecting reference stations for evaluating urbanization effect on surface air temperature trends. *J. Climate*, **24**, 3179–3189, doi:10.1175/2010JCLI3658.1.

Ren, Z., and A. Xiong, 2007: Operational system development on three-step quality control of observation from AWS. *Meteor. Mon.*, **33**, 19–24.

——, and Coauthors, 2015: Development of three-step quality control system of real-time observation data from AWS in China. *Meteor. Mon.*, **41**, 1268–1277.

Rosenfeld, D., 1999: TRMM observed first direct evidence of smoke from forest fires inhibiting rainfall. *Geophys. Res. Lett.*, **26**, 3105–3108, doi:10.1029/1999GL006066.

——, 2000: Suppression of rain and snow by and industrial urban air pollution. *Science*, **287**, 1793–1796, doi:10.1126/science.287.5459.1793.

——, U. Lohmann, G. B. Raga, C. D. O'Dowd, M. Kulmala, S. Fuzzi, A. Reissell, and M. O. Andreae, 2008: Flood or drought: How do aerosols affect precipitation? *Science*, **321**, 1309–1313, doi:10.1126/science.1160606.

Rosenzweig, C., W. D. Solecki, L. Parshall, M. Chopping, G. Pope, and R. Goldberg, 2005: Characterizing the urban heat island in current and future climates in New Jersey. *Environ. Hazards*, **6**, 51–62, doi:10.1016/j.hazards.2004.12.001.

Rozoff, C. M., W. R. Cotton, and J. O. Adegoke, 2003: Simulation of St. Louis, Missouri, land use impacts on thunderstorms. *J. Appl. Meteor.*, **42**, 716–738, doi:10.1175/1520-0450(2003)042<0716:SOSLML>2.0.CO;2.

Seto, K., and J. M. Shepherd, 2009: Global urban land-use trends and climate impacts. *Curr. Opin. Environ. Sustain.*, **1**, 89–95, doi:10.1016/j.cosust.2009.07.012.

Shastri, H., S. Paul, S. Ghosh, and S. Karmakar, 2015: Impacts of urbanization on Indian summer monsoon rainfall extremes. *J. Geophys. Res. Atmos.*, **120**, 495–516, doi:10.1002/2014JD022061.

Shepherd, J. M., and S. J. Burian, 2003: Detection of urban-induced rainfall anomalies in a major coastal city. *Earth Interact.*, **7**, doi:10.1175/1087-3562(2003)007<0001:DOUIRA>2.0.CO;2.

——, M. Carter, M. Manyin, D. Messen, and S. Burian, 2010: The impact of urbanization on current and future coastal precipitation: A case study for Houston. *Environ. Plann. Plann. Des.*, **37**, 284–304, doi:10.1068/b34102t.

Song, X. and Coauthors, 2014: Rapid urbanization and changes in spatiotemporal characteristics of precipitation in Beijing metropolitan area. *J. Geophys. Res. Atmos.*, **119**, 11 250–11 271, doi:10.1002/2014JD022084.

Stewart, I. D., and T. R. Oke, 2012: Local climate zones for urban temperature studies. *Bull. Amer. Meteor. Soc.*, **93**, 1879–1900, doi:10.1175/BAMS-D-11-00019.1.

Sun, J. S., and W. J. Shu, 2007: Impact of UHI effect on winter and summer precipitation in Beijing City. *Atmos. Sci.*, **31**, 311–320.

Thielen, J., W. Wobrock, A. Gadian, P. G. Mestayer, and J. D. Creutin, 2000: The possible influence of urban surfaces on rainfall development: A sensitivity study in 2D in the meso-γ-scale. *Atmos. Res.*, **54**, 15–39, doi:10.1016/S0169-8095(00)00041-7.

Wu, X., X. Wang, X. Zeng, and L. Xu, 2000: The effect of urbanization on short duration precipitation in Beijing. *J. Nanjing Inst. Meteor.*, **23**, 69–72.

Yang, P., and W. D. Liu, 2013: Evaluating the quality of meteorological data measured at automatic weather stations in Beijing during 1998–2010. *Adv. Meteor. Sci. Technol.*, **3**, 27–34.

——, ——, J. Zhong, and J. Yang, 2011: Evaluating the quality of temperature measured at automatic weather stations in Beijing. *J. Appl. Meteor. Sci.*, **22**, 706–715.

——, W. Hou, and G. Feng, 2012: The characteristics of clusters in weather and climate extreme events over China in recent 50 years. *Chin. Phys.*, **21 B**, 019201, doi:10.1088/1674-1056/21/1/019201.

——, G. Ren, W. Hou, and W. Liu, 2013a: Spatial and diurnal characteristics of summer rainfall over Beijing municipality based on a high-density AWS dataset. *Int. J. Climatol.*, **33**, 2769–2780, doi:10.1002/joc.3622.

——, ——, and W. Liu, 2013b: Spatial and temporal characteristics of Beijing urban heat island intensity. *J. Appl. Meteor. Climatol.*, **52**, 1803–1816, doi:10.1175/JAMC-D-12-0125.1.

——, Z. N. Xiao, J. Yang, and H. Liu, 2013c: Characteristics of clustering extreme drought events in China during 1961–2010. *Acta Meteor. Sin.*, **27**, 186–198, doi:10.1007/s13351-013-0204-x.

——, ——, and W. Shi, 2017: Fine-scale characteristics of rainfall in Beijing urban area based on a high-density AWS dataset. *Chin. J. Atmos. Sci.*, **41**, 475–489, doi:10.3878/j.issn.1006-9895.

Yu, R., X. Yu, T. Zhou, and J. Li, 2007: Relation between rainfall duration and diurnal variation in the warm season precipitation over central eastern China. *Geophys. Res. Lett.*, **34**, L13703, doi:10.1029/2007GL030315.

Zhan, J., J. Huang, T. Zhao, X. Geng, and Y. Xiong, 2013: Modeling the impacts of urbanization on regional climate change: A case study in the Beijing–Tianjin–Tangshan metropolitan area. *Adv. Meteor.*, **2013**, 849479, doi:10.1155/2013/849479.

Zhang, C. L., F. Chen, S. G. Miao, Q. C. Li, X. A. Xia, and C. Y. Xuan, 2009: Impacts of urban expansion and future green planting on summer precipitation in the Beijing metropolitan area, *J. Geophys. Res.*, **114**, D02116, doi:10.1029/2008JD010328.

Zhang, N., Z. Gao, X. Wang, and Y. Chen, 2010: Modeling the impact of urbanization on the local and regional climate in Yangtze River Delta, China. *Theor. Appl. Climatol.*, **102**, 331–342, doi:10.1007/s00704-010-0263-1.

Zhang, Y., J. A. Smith, L. Luo, Z. Wang, and M. L. Baeck, 2014: Urbanization and rainfall variability in the Beijing metropolitan region. *J. Hydrometeor.*, **15**, 2219–2235, doi:10.1175/JHM-D-13-0180.1.

Zhong, S., Y. Qian, C. Zhao, R. Leung, and X. Yang, 2015: A case study of urbanization impact on summer precipitation in the Greater Beijing Metropolitan Area: Urban heat island versus aerosol effects. *J. Geophys. Res. Atmos.*, **120**, 10 903–10 914, doi:10.1002/2015JD023753.

Zhou, Y., and G. Ren, 2009: The effect of urbanization on maximum, minimum temperature and daily temperature range in north China. *Plateau Meteor.*, **28**, 1158–1166.